X-ray/Hα scaling relationships in stellar flares

Hiroki KAWAI[*a], Yohko TSUBOI[*a], Wataru B. IWAKIRI[a,b], Yoshitomo MAEDA[c], Satoru KATSUDA[d], Ryo SASAKI[a], Junya KOHARA[a], the MAXI TEAM

[a]*Department of Physics, Chuo University, 1-13-27 Kasuga, Bunkyo-ku, Tokyo 112-8551, Japan,*
[b]*RIKEN, 2-1 Hirosawa, Wako, Saitama 351-0198, Japan,*
[c]*Institute of Space and Astronautical Science, Japan Aerospace Exploration Agency, 3-1-1 Yoshinodai, Chuo-ku, Sagamihara, Kanagawa 252-5258, Japan,*
[d]*Graduate School of Science and Engineering, Saitama University, 255 Shimo-Okubo,Sakura, Saitama, 338-5670, Japan,*

Abstract

We report on the results of our simultaneous observations of three large stellar flares with soft X-rays (SXRs) and an Hα emission line from two binary systems of RS CVn type. The energies released in the X-ray and Hα emissions during the flares were 10^{36}–10^{38} and 10^{35}–10^{37} erg, respectively. This renders the set of the observations as the first successful simultaneous X-ray/Hα observations of the stellar flares with energies above 10^{35} erg; although the coverage of the Hα observations of the stellar flares with energies above 10^{35} erg; although the coverage of the Hα observations was limited, with ~10% of the e-folding time in the decay phase of the flares, that of the SXR ones was complete. Combining the obtained physical parameters and those in literature for solar and stellar flares, we obtained a good proportional relation between the emitted energies of X-ray and Hα emissions for a flare energy range of 10^{29}–10^{38} erg. The ratio of the Hα-line to bolometric X-ray emissions was ~0.1, where the latter was estimated by converting the observed SXR emission to that in the 0.1–100 keV band according to the best-fitting thin thermal model. We also found that the e-folding times of the SXR and Hα light curves in the decaying phase of a flare are in agreement for a time range of 1–10^4 s. Even very large stellar flares with energies of six orders of magnitude larger than the most energetic solar flares follow the same scaling relationships with solar and much less energetic stellar flares. This fact suggests that their physical parameters can be estimated on the basis of the known physics of solar and stellar flares.

1. Introduction

Large stellar flares with energies between 10^{34}–10^{39} erg have been detected (Tsuboi et al., 2016; Sasaki et al., 2021) with the all-sky X-ray monitor, Monitor of All-sky X-ray Image (MAXI Matsuoka et al., 2009) since its launch in 2009. The majority of the detected flares are estimated to have loop lengths likely larger than the radii of their host stars by a factor of ~5.

The MAXI-detected flares have extremely large energy-related parameters: luminosities of 10^{31-34} erg s^{-1} in the 2–20 keV band, emission measures of 10^{54-57} cm^{-3}, e-folding times of 1 hr to 1.5 d, and total radiative energies of 10^{34-39} erg. Tsuboi et al. (2016) found a universal correlation between the flare duration and peak X-ray luminosity, combining the X-ray flare data of nearby stars and the Sun. Moreover, they found that the MAXI-detected flares extended the established correlation between the flare-peak emission measure and temperature for solar flares and small stellar ones (Shibata and Yokoyama, 1999). Given that the correlations hold over a broad range of energies from solar micro flares to large stellar flares, the correlation suggests the presence of some common mechanism governing flare-loop formation and its cooling processes.

One of the other important observational probes for flare physics is the Hα emission. In the solar flare, Hα is known to be emitted from the foot of the loop, called the "Hα Ribbon", and/or a loop located at the inner side of a soft X-ray (hereafter, SXR) flare loop, called a postflare loop (see figure 42 in Shibata and Magara, 2011). Since the emission region and mechanism are different from those of the SXR, the information obtained from the Hα emission is complementary to that from the SXR emission. Hence, the study of the relationship between the SXR and Hα flares from distant stars, where imaging observations are difficult unlike the Sun, can provide key information about the overall geometrical structure and evolution mechanism of stellar flares.

Butler et al. (1988) and Butler (1993) derived a positive relation between the emitted energies with the Hγ emission line and SXR. Veronig et al. (2002a) performed a detailed study of solar flares and reported on a positive relation between the decay times (e-folding times) of the observed fluxes of the Hα line and SXR. However, no studies have ever been conducted about samples containing very large stellar flares, the energy of which can reach orders of magnitude larger than that of the largest solar flares, such as those detected with MAXI. Consequently, whereas physics of solar flares is comparatively well understood, our understanding of flare physics of much larger or more active stars than the Sun remains poor and not much

more than speculation.

Here we report on the results of our Hα observations (see section 2 for the observation details) conducted immediately after after triggers of MAXI detection of large stellar flares with emitted energies of up to 10^{38} erg, combining the simultaneous observations with MAXI (section 2) and continuous Hα monitoring. Specifically, we focus on three flares with the best statistics and analyze them via the methods described in section 3. These are the first simultaneous observational samples ever reported of the Hα and SXR emissions of stellar flares with energies over 10^{35} erg, which is the previous record (a flare from II Peg reported by Butler, 1993). Then we investigate the relations of the energy and e-folding time between the Hα and SXR emissions and discuss them (section 4) before summarizing our result in section 5.

2. Observations

2.1. MAXI

SXR is taken with the Monitor of All-sky X-ray Image, MAXI (Matsuoka et al., 2009) . MAXI is an astronomical X-ray observatory mounted on the International Space Station (ISS). In this analysis, we used data from the Gas Slit Camera (Mihara et al., 2011), which is sensitive in the 2–30 keV band. It consists of 12 proportional counters, each of which employs carbon-wire anodes to provide one-dimensional position sensitivity. A pair of counters form a single camera unit; hence the instrument consists of six camera units. The six camera units are assembled into two groups whose fields of view (FoVs) are pointed toward the tangential direction of the ISS motion along the earth horizon and the zenith direction. The FoVs are $160° \times 3°$, which corresponds to 2% of the whole sky. These counters are not operated in the regions with high particle background, such as the South Atlantic Anomaly and at absolute latitudes higher than ∼ 40°, or in the vicinity of the Sun (within ∼ 5°). Hence the Gas Slit Camera has an operating duty ratio of ∼ 40% and scans about 85% of the whole sky per orbit of the ISS. The time interval of MAXI observations is ∼92 min, which is the same as the orbital period of the ISS. The exposure time of a target is ∼50 s per orbit.

2.2. SCAT

The Spectroscopic Chuo-university Astronomical Telescope (SCAT; figure 1) is a MEADE 36 cm diameter optical telescope built on the rooftop of a building on the campus of Chuo University, situated in downtown of Tokyo, Japan (latitude = 35°42′30″N, longitude = 139°44′54″E). SCAT is equipped with an ATIK 460EX CCD camera with a Shelyak Alpy 600 spectrometer, suitable for low-resolution spectroscopic observations of the Hα emission line. The spectrometer covers wavelengths of 3700 to 7500 Å with a spectral resolution of $R = 600$. SCAT has the limiting magnitude at 6000 Å of about 10 mag. Its signal-to-noise ratio is 10 for an exposure of 600 s. SCAT observes the sky when the elevation is larger than 30°. This means that an area of the sky with a declination angle of larger than −20° is observable.

Figure 1: SCAT and its basic performance. Mirror–MEADE F8ACF35 (356 mmφ, FL 2845 mm). Equatorial mount–Takahashi EM-400 Temma2Z. Finder–WAT-910HX/RC, CBCM5018-MP2 (50 mm). Grating–Shelyak Alpy 600 (Resolution power $R = 600$). Sensor–ATIK 460EX. Sensitivity–10 mag for 600s exposure. Band width–3700–7400 Å.

2.3. Simultaneous observations

Table 1: Time history of our simultaneous observations

Flare ID	Nova alert (MJD)	SXR peak time (MJD)	Start time of the SCAT observation (MJD)
Flare 1	57714.1651	57714.2612	57714.4163
Flare 2	58446.7929	58446.7587	58447.4228
Flare 3	58157.9849	58158.0790	58158.3802

We made use of "nova alerts" (Negoro et al., 2016) to do follow-up observations of MAXI-detected stellar flares. A time history of the nova alerts of three selected flares along with the SXR flare peak and the start time of the Hα emission is shown in Table 1. The flare peaks of Flares 1, 2, and 3 appeared about +0.10, −0.04, and −0.09 d, respectively, after the corresponding nova alert. This automated alert system identifies X-ray transients from the image taken in real time, and classifies them into four types of events: "Burst", "Alert", "Warning", and "Info". While "Burst" is automatically reported to scientists across the world via the "MAXI Mailing List (MAXI ML)", "Alert" and "Warning" are examined by duty scientists before a notification is circulated to MAXI ML. We started follow-up observations with SCAT, immediately after receiving a signal from "nova alerts" as duty scientists of MAXI. The detections of all the MAXI flares which we work on or mention in this paper (seven flares) were circulated to the MAXI ML.

Apart from the flare periods, SCAT regularly monitored the sources, and the data were used to identify their characteristics during the persistent phase. The sources were selected from the MAXI-detected flare sources (e.g., Sasaki et al. 2017).

During the period between 2016 November and 2021 October, we successfully made SCAT observations of seven stellar flares to follow up MAXI-alerted events. Out of the seven flares, we selected three flares for our analysis presented in this paper via the following criteria. First, the X-ray data of the flare must have sufficient statistics to determine the *e*-folding time (accordingly, Flare 5 was excluded; see Appendix Appendix A). Secondly, the decay phase of the flare must have been observed with SCAT (Flares 6 and 7 thus excluded)[1]. Thirdly and lastly, Flare 4, which showed clear multiple peaks in the SCAT light-curve, was excluded because our analysis relies on a simple-profile light curve in the decaying phase. The three selected flares are referred to as Flares 1, 2, and 3. Flares 1 and 2 occurred at UX Ari whereas Flare 3 did so at AR Psc. The detection history is listed in table 1.

2.4. Objects

2.4.1. UX Ari

UX Arietis (UX Ari, HD 21242, HIP 16042) is a binary system of RS CVn type (Fekel et al., 1986), located at a distance of 50.2 pc (ESA, 1997). It consists of a primary K0 subgiant and a secondary G5 main-sequence star. The synchronous rotation period is reported to be 6.43791 ± 0.00006 d (Carlos and Popper, 1971). The CHARA six-telescope optical long-baseline array revealed that its spots can fill about 62% of the primary surface (Hummel et al., 2017). Hummel et al. (2017) reported that the radii of the primary and secondary stars are 5.6 ± 0.1 R$_\odot$ and 1.6 ± 0.2 R$_\odot$, respectively, with an inclination angle of $125°.0 \pm 0°.5$ and a separation of 18.8 ± 0.1 R$_\odot$ (table 2).

UX Ari has been known as a very active flare-star binary (Feldman, 1978; Tsuru et al., 1989; Massi et al., 1998; Massi and Ros, 2002; Catalano et al., 2003; Massi et al., 2005; Peterson et al., 2011). Tsuboi et al. (2016), Matsumura et al. (2011), and Kawagoe et al. (2014) detected large flares with luminosities of 2×10^{32} erg s^{-1} or larger, using MAXI.

Table 2: General properties of UX Ari

Parameters	Primary	Secondary	References[*]
Sp. type	K0IV	G5V	(1)
Radius [R$_\odot$]	5.6 ± 0.1	1.6 ± 0.2	(2)
Separation [mas]	1.750 ± 0.01		(2)
Separation [R$_\odot$]	18.8 ± 0.1		(2)(3)
Distance [pc]	50.2		(3)
Orbital period [d]	6.43791 ± 0.00006		(1)
Inclination [degree]	125.0 ± 0.5		(2)

*(1)Carlos and Popper (1971); (2)Hummel et al. (2017);
(3)ESA (1997).

[1]We did make Hα observations during the period at around their flare peaks but not in their decay phases due to bad weather.

2.4.2. AR Psc

AR Psc (= HD 8357 = BD +06 211) is a binary system of RS CVn type (Fekel, 1996), located at a distance of 45.9 pc (Gaia Collaboration et al., 2018). It consists of a primary K1 subgiant and a secondary G7V dwarf. The projected rotational velocity ($v \sin i$) of the AR Psc primary is 6.5 ± 2 km s^{-1} whereas the orbital period is 14.3023 d (Fekel, 1996). AR Psc is an active binary in Hα emission (Fekel, 1996). Fekel et al. (1986) found that the Hα emission is mostly associated with the component originating from the primary star, although that from the secondary has a weak contribution to it, as seen in the combined spectrum. AR Psc is also known to be active in the X-ray band (Garcia et al., 1980; Kashyap and Drake, 1999; Shan et al., 2006). Nakamura et al. (2016) reported on a flare detection by MAXI, revealing a large activity in X-ray flares.

3. Analysis & Results

3.1. Soft X-Ray (SXR) emission

The MAXI on-demand system (Nakahira et al., 2013) was used for obtaining light curves and spectra. The source photons were extracted from a circular region with a radius of $1°.5$ centered on each target, i.e., UX Ari and AR Psc, the area of which corresponds to the point-spread function of the detector (Gas Slit Camera) of MAXI. The background photons were extracted from an annular region with inner and outer radii of $1°.5$ and $4°.0$, respectively, centered at the source position.

We fitted an exponential model to the light curve of each flare and derived the decay timescale. The time range used for the fitting of each light curve is shown with a black, horizontal arrow in figure 2. In the light curves, Flares 2 and 3 may have secondary peak. Then, we fitted the X-ray light curves, limiting the time region for only ~2 d from the flare peak (see figure 2) to avoid possible contamination by a potential secondary peak, which may appear then. Table 3 lists the fitting results, including the *e*-folding time, τ.

Table 3: Flare *e*-folding time τ.[*]

Flare ID		Region of interest [d] / [10^4 s]	τ [10^4 s]	Reduced χ^2 (d.o.f.)
Flare 1	SXR	1.9 / 16	2 (1–4)	0.3 (9)
	Hα	0.5 / 4.3	8 (7–10)	0.6 (11)
Flare 2	SXR	1.9 / 16	7 (5–10)	0.2 (3)
	Hα	0.4 / 3.5	24 (19–32)	0.8 (22)
Flare 3	SXR	1.5 / 13	3 (2–5)	0.8 (2)
	Hα	0.08 / 0.69	7 (4–17)	0.4 (8)

[*] In the 2–10 keV band for SXR. The errors are 90% confidence range. "d.o.f." means the degree of freedom.

The source spectrum during each flare was extracted from the data of the time bin for the peak flux in each flare (figure 2) and the background component, accumulated from the above-mentioned annular region, is subtracted from it. The latter represents the sum of the instrumental and sky background components. Figure 3 shows the resultant flare spectra. Although
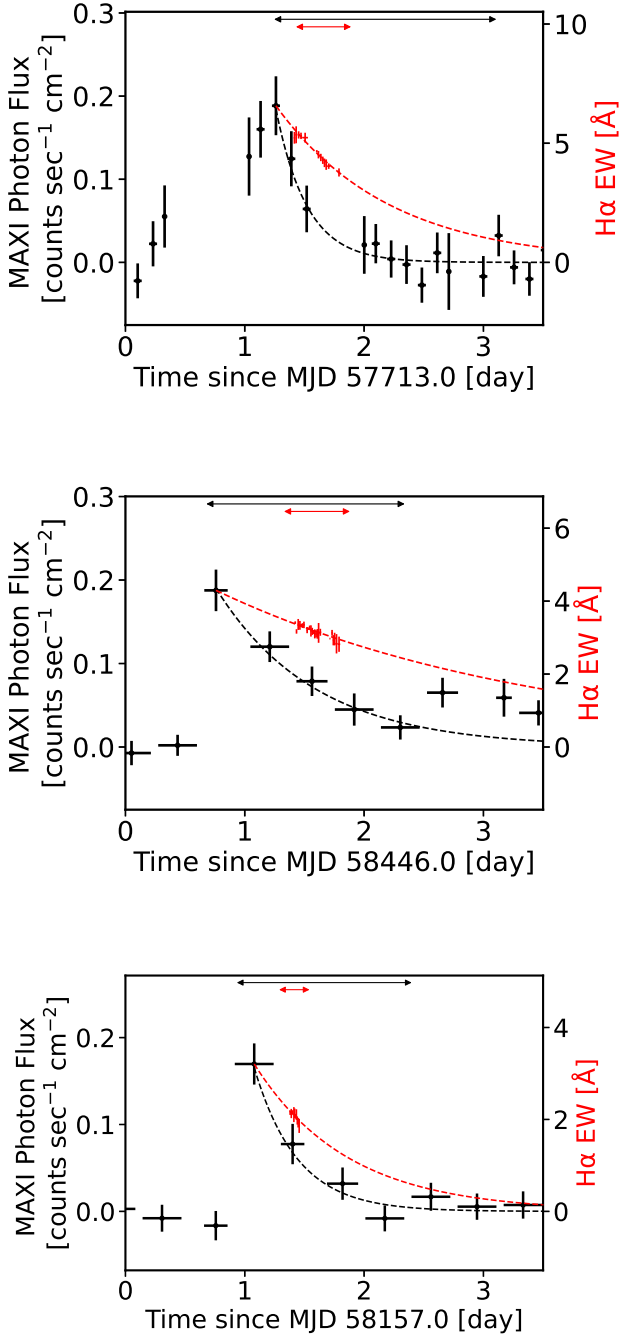
Figure 2: SXR and Hα light curves of the Flare 1 (upper panel), Flare 2 (middle), and Flare 3 (lower). The instrumental background (see Section 3.1) is subtracted in the presented SXR light curves. The SXR in the 2–10 keV band, overlaid with its best-fitting model, is plotted in black, with 1 σ error, with bins for 2, 6, and 6 MAXI orbital periods in the respective three panels. The time range used for the fitting of each of the SXR and Hα light curves is indicated with horizontal arrows in black and red, respectively, at the top of each panel. Hα EW is presented in red with 90% error bar for the data and best-fitting model.

the spectra contain the quiescent component, the contribution is negligible; Webb et al. (2020) presented the catalog of active stars, including our targets, UX Ari and AR Pic, which contains the quiescent fluxes of the sources. Their flux levels are ∼3% or lower of any peak fluxes of the flares we reported here.

We fitted the spectra with a thin thermal plasma model, APEC (Smith et al., 2001) in the Xspec package, where the redshift and metal abundace were fixed to 0 and 0.3, respectively. In the fitting, as for Flares 1 and 2, we fixed the temperature kT to the average value according to Tsuboi et al. (2016) because otherwise no meaningful constraints would be obtained due to poor data statistics. Table 4 lists the fitting results and figure 3 shows the best-fitting models. Then, the radiation energies were calculated, from the best-fitting e-folding timescale and the luminosity, and are given in table 5.

Table 4: SXR best-fitting spectral parameters.[*]

Flare ID	kT [keV]	Emission measure [10^{55} cm^{-3}]	Reduced χ^2 (d.o.f.)
Flare 1	3.5[†]	5 (3–6)	0.1 (4)
Flare 2	3.5[†]	4 (3–5)	1.7 (8)
Flare 3	3 (2–6)	4 (3–7)	0.8 (6)

[*] Abundance and redshift are fixed at 0.3 and 0, respectively. The errors indicate a 90% confidence range. "d.o.f". means the degree of freedom.
[†] kT is fixed according to Tsuboi et al. (2016) (see text for detail).

3.2. Hα emission

We derived the flux of the Hα emission line for each flare as follows. In general, the direct measurement of the flux of optical grating data is known to be very difficult due to unstable pointing of a telescope and/or weather condition. Hence, we instead derived an equivalent width (EW) of Hα first. Then we converted the Hα EW to its flux.

To obtain the EW of the Hα emission line, we took each frame of the SCAT observations of UX Ari and AR Psc with the exposure of 300 s. Also, we took the frame of 73 Cet (HD 15318) and 2 Ori (HD 30739) in the same way as the standard stars for UX Ari and AR Psc, respectively, for photometric corrections. We reduced the SCAT data frame-by-frame with a standard manner in Python's astronomical packages. These reductions are all common among the observations of the flare sources in both flare phases and quiescent phases.

Figure 4 shows an example of spectra during flare phase and quiescent phase, but normalized at 6,600Å. We applied a standard technique to our spectra and derived the EW. We fitted the Hα emission line with a Gaussian, and picked up the ±3σ points from the Gaussian peak as the "edge" between the emission line and continuum emission (figure 4). As for the Hα line intensity, we integrated the data above the linear function which connects both sides of the "edge". As for the continuum level, we took the value of the linear function, just at the center of the

Table 5: Summary of the three flares.

| Flare ID | Star | Flare peak time | | Wavelength | Peak luminosity[†] $[10^{32}$ erg s$^{-1}]$ | Energy[†] $[10^{36}$ erg$]$ |
		UT	MJD			
Flare 1	UX Ari	2016/11/22 06:16	57714.2612	SXR	3 (2–4)	6 (2–12)
				Hα	0.13 (0.06–0.20)	1.1 (0.5–1.7)
Flare 2	UX Ari	2018/11/24 18:12	58446.7587	SXR	3 (2–4)	20 (10–30)
				Hα	0.08 (0.04–0.12)	1.9 (0.9–3.0)
Flare 3	AR Psc	2018/02/09 01:53	58158.0790	SXR	2.5 (1.4–3.1)	8 (3–13)
				Hα	0.04 (0.02–0.07)	0.3 (0.1–0.8)

[*] In the 2–10 keV band for SXR.
[†] The errors are 90% confidence range. The Hα luminosities represent the values extrapolated to the times of the X-ray peak times. The errors for the Hα luminosities and radiated energies include the uncertainties in determining the decay times.

Gaussian. We then divided the integrated Hα line intensity by the continuum level, and finally obtained the EW.

Since UX Ari and AR Psc had orbital variation in EW during the quiescent phase, we needed to determine the curve to subtract the orbital variation. We first folded their light curves, in the quiescent phase, with the rotation period P_{rot}, and fitted it with a function of $a\sin[(x-b)/P_{rot}]+C$, and determined the EW in each orbital phase. Table 6 lists the best-fitting values of a, b, and C. The value of the EW curve at the same orbital phase was then subtracted from that during the flare and was defined as the EW of the flare. Here, many past optical observations of solar and stellar flares show no large change in continuum flux (e.g. Namekata et al., 2020). We then assume that the continuum flux of our observations did not change from the quiescent to the flare phase. The fact that no significant variation was found for the continuum flux in the band adjacent to the Hα line supports the assumption. As a result, the Hα EW is basically proportional to the flux of the band where the line component dominates. The resultant curve for the EW is plotted in figure 2.

We fitted the Hα light curves with an exponential function in the same manner for the SXR light curves. Table 3 lists the fitting result. Here, as for the Hα light curve of Flare 1, we performed fitting for the time region of the first day of the flare peak only, during which an enhancement in emission was apparent. We note that the inclusion of the data in the second observation period (on the fourth day) in the fitting yielded the best-fitting decay time of 9.9 (9.5–10.4) $\times 10^4$ s, which is not significantly different from the original result of 8 (7–10) $\times 10^4$ s (table 3); in other words, the selection of the time region between the two for the fitting has no significant influence on the result.

In order to obtain the released energy during a flare as the Hα line emission, we needed to estimate the peak Hα intensities, although they are not covered in our follow-up observations. Then, we needed to extrapolate the best-fitting function to the flare-peak epoch obtained in the SXR light curve. We note that it should be a reasonable assumption, given that the coincidence of the SXR and Hα peaks have been reported from the data of roughly 200 solar flares (Veronig et al., 2002b) as well as from stellar flares (Doyle et al., 1988a; Fuhrmeister et al., 2011; Namekata et al., 2020), and also that the calculated total radiated energy is not very sensitive to the model shape (e.g.,

whether it is an e-folding decay as we employed or two-peak decay, which may be the case in some flares) that is applied to approximate the light curve.

We calculated the Hα peak luminosity by extrapolating the time-profile of the observed Hα EW to the X-ray peak time, subtracting the averaged continuum level during a one-night observation, and using the distance to the object. The absolute flux measurements of continuum emission is in general known to be very difficult for the spectroscopic data that we took. The continuum level of our data was actually fluctuated in 50% at 90% error. We then gave this error to the Hα flux of our measurements. Table 5 shows the results, where the uncertainties in determining the decay times are taken into account in the calculation of the errors.

Table 6: EW of Hα during the quiescent phase.

Flare ID	Star[*]	Observation dates	a[†]	b[†]	C[†]
Flare 1	UX Ari	2016 Oct – 2017 Mar	1.0	0.3	0.6
Flare 2	UX Ari	2018 Sep – 2019 Apr	−0.2	0.0	0.4
Flare 3	AR Psc	2016 Oct – 2017 Feb, 2018 Feb	0.4	0.2	0.1

[*]UX Ari and AR Psc observations folded with ephemerides MJD = 45695.6142 and 46079.450, respectively (Alekseev, 2014; Carlos and Popper, 1971; Fekel, 1996). [†]We fitted the light curve to a function of $a\sin[(x-b)/P_{rot}]+C$.

4. Discussion

4.1. Flare loop

We determined loop lengths of flares, using the "kT-EM diagram" model formulated by Shibata and Yokoyama (1999), where the pre-flare electron density was assumed to be 10^9 cm^{-3}. Independently, we also derived the same parameters, using the model formulated by Haisch (1983). The estimated loop lengths based on the former model were roughly three times larger than the binary separation for Flares 1 and 2, whereas those based on the latter model are comparable to the binary separation. Table 7 summarizes the result.

4.2. Radiation energy

Butler et al. (1988) presented the linear relationship between the radiation energy of flares in the Hγ emission line ($E_{H\gamma}$) and

Table 7: Loop lengths of the three flares.

	Loop lengths[*]			
	(Shibata and Yokoyama, 1999)		(Haisch, 1983)	
Flare ID	[$R_\odot$]	(Binary separation)	[$R_\odot$]	(Binary separation)
Flare 1	62 (51–74)	3.3 (2.7–3.9)	11 (7–16)	0.6 (0.4–0.9)
Flare 2	57 (50–67)	3.1 (2.7–3.6)	25 (20–32)	1.3 (1.1–1.7)
Flare 3	80 (30–220)	–	14 (10–19)	–

[*]The errors indicate the 90% confidence range.

that in the X-ray band in the 0.04–2 keV band. Butler (1993) further extended the relation in energy to the range of seven orders of magnitude: 10^{29}–10^{36} erg [2].

We produce the same kind of plot, the radiation energy of flares in the Hα emission line ($E_{\mathrm{H}\alpha}$) vs. that in the X-ray bolometric band (E_{Xbol}), in Figure 5, incorporating past studies from literature (Butler, 1993; Butler et al., 1988; Thomas and Teske, 1971; Kahler et al., 1982; Butler et al., 1986; Doyle et al., 1988b,a, 1991; Johns-Krull et al., 1997). In deriving the total $E_{\mathrm{H}\alpha}$ energy, some of the past reports used in the compilation presented the radiation energy in the Hγ emission ($E_{\mathrm{H}\gamma}$) only and no $E_{\mathrm{H}\alpha}$; we estimated the latter from the former according to the assumed relation $E_{\mathrm{H}\alpha} = 2 \times E_{\mathrm{H}\gamma}$ in such cases, as Butler (1993) converted the latter to the former using the same conversion factor. As for the total SXR energy, the flare parameters measured in SXR are converted to those in the bolometric energy band (0.1–100 keV band), using the same method described in Tsuboi et al. (2016); the peak bolometric luminosities were obtained, integrating the best-fitting spectral parameters with a thin-thermal plasma model for a range of 0.1–100 keV, and then the bolometric X-ray energies E_{Xbol} were calculated from it multiplied by its e-folding times. Table 8 summarizes the compiled parameters for the stellar flares. Appendix B gives a detailed description about the conversion methods for some of the values in table 8 taken from literature.

Fitting all the data points with a linear model with a slope of unity yields the best-fitting relation of

$$\log E_{\mathrm{H}\alpha} = 1 \log E_{\mathrm{Xbol}} - 1.0 \pm 0.7 \ , \qquad (1)$$

which is shown in figure 5. The error ±0.7 is calculated as the scatter of the data points around the derived model function in 1.6σ.

Our result finds that the applicable range of the relation extends for a further two orders in energy, 10^{29}–10^{38} erg. The scattering of the data around the best-fitting linear function is limited within an order.

[2]The "integrated flux" with the notations L_{X} and $L_{\mathrm{H}\gamma}$ in Butler et al. (1988); Butler (1993) should be interpreted as, though not explicitly explained in their papers, the radiated energy *integrated over the flare duration*. This means that its dimension is energy (erg), as opposed to the nominally expected units of energy per unit time (erg s^{-1}) for L_*. See the definitions of the parameters in e.g., Thomas and Teske (1971), from which Butler (1993) adopted the values, for verification.

4.3. e-folding time

The SXR light curve has limited photon statistics whereas the Hα light curve covers a limited period during each flare (figure 2). Both limitations contribute to the uncertainty in the e-folding times that we derived in section 3.

As for the SXR, the light curves of some large flares have been shown to contain two components with different e-folding times (e.g. Agrawal and Vaidya, 1988; Tsuboi et al., 1998). The decay time of the component that is dominant near the peak is reportedly shorter than the one dominant at the tail. Tsuru et al. (1989) reported re-heating or a second flare at the tail of the first and main component in a flare of UX Ari. The decay time that we derived is similar to that of the main flare component ($\sim 6.5 \times 10^4$ s) seen in their lightcurve. Flare 2 might actually be a double flare similar to the one reported by Tsuru et al. (1989), i.e., the SXR light curve of Flare 2 might involve a peak of a possible second flare at around 2 d after the first peak.

With the optical continuum band, intensive studies of flare decay timescales have been made for solar flares. For example, Kashapova et al. (2021) reported two decay components, of which the slower-decay component lasts longer by a factor of 2–10 than the faster-decay one. Our data of Hα covered a small fraction of the flare decay phase, suggesting that we only detected one component out of possibly two or more components in reality in the light curves. Therefore, we conclude that the best-fitting e-folding times of the SXR and Hα emissions that we measured with the single-exponential model fitting has a (systematic) error of a factor of 2–10 and thus is robust in only one order of accuracy.

Many studies of stellar flares (e.g., Kashapova et al., 2021) show that faster and slower decaying components have high and low peak fluxes, respectively. Then, the flare energy that is determined from the decay time multiplied by the peak luminosity is not varied much because the uncertainties compensate each other, if to a certain degree.

Veronig et al. (2002a) found a linear correlation between the e-folding times τ_{SXR} and $\tau_{\mathrm{H}\alpha}$ for solar flares. In Figure 6, we compiled the same kind of plot, but incorporating the data for stellar flares as in the previous subsection. Here, the reported e-folding times were adopted as they are, regardless of the energy band used in each study. The linear relationship is again apparent in this figure. We then fitted the plot with a linear function. The best-fit model, which is overlaid in figure 6, is given by

$$\log \tau_{\mathrm{H}\alpha} = 1 \log \tau_{\mathrm{SXR}} - 0.1 \pm 0.6 \ , \qquad (2)$$

Table 8: SXR and Hα radiation energy and *e*-folding time of large flares.[*]

Star	log (E_Xbol [erg])	log ($E_{\mathrm{H}\alpha}$ [erg])	log (τ_SXR [s])	log ($\tau_{\mathrm{H}\alpha}$ [s])	References[†]
UX Ari	37.1 (36.7–37.5)	36.0 (35.7–36.2)	4.4 (4.1–4.6)	4.91 (4.86–4.98)	This work (Flare 1)
	37.6 (37.3–37.8)	36.3 (35.9–36.5)	4.9 (4.7–5.0)	5.4 (5.3–5.5)	This work (Flare 2)
AR Psc	37.2 (36.7–37.5)	35.5 (35.0–35.9)	4.5 (4.3–4.7)	4.8 (4.6–5.2)	This work (Flare 3)
II Peg	35.6	34.0[‡]	3.6	3.7[‡]	(1), (2)
Gliese 644	33.3	31.8	3.0	3.3	(3)
YZ CMi	31.0	30.0[‡]	2.4	2.0[‡]	(4)
	31.7	31.0[‡]	2.7	2.4[‡]	(5)
UV Cet	29.8	29.0[‡]	2.0	2.4[‡]	(6), (7)
	30.5	29.2[‡]	2.4	2.4[‡]	(6), (7)
	29.8	28.9[‡]	2.4	2.4[‡]	(6), (7)
	30.8	29.6[‡]	3.0	2.7[‡]	(6), (7)
Sun	29.1	28.0	3.3	2.7	(8)
	29.5	28.8	3.3	2.9	(8)
	29.8	29.0	3.3	2.7	(8)
	30.0	29.6	3.6	3.3	(8)
	30.2	29.8	3.6	3.1	(8)
	30.6	30.0	3.6	3.1	(8)
	31.0	30.7	3.9	3.7	(8)
	31.9	30.8	3.9	3.8	(8)
	31.2	29.7	3.5	3.5	(9)

[*]The errors indicate the 90%-confidence range. See Appendix B for the detailed method of the calculation. The energy band of E_Xbol is 0.1–100 keV.

[†](1) Butler (1993), (2) Doyle et al. (1991), (3) Doyle et al. (1988b), (4) Doyle et al. (1988a), (5) Kahler et al. (1982), (6) Butler et al. (1986), (7) Butler et al. (1988), (8) Thomas and Teske (1971), (9) Johns-Krull et al. (1997)

[‡]$E_{\mathrm{H}\alpha} = 2E_{H\gamma}$ and $\tau_{\mathrm{H}\alpha} = \tau_{\mathrm{H}\gamma}$ are assumed.

Figure 4: Normalized spectra in a wavelength range at around the Hα emission line. The solid and dashed lines correspond to Flare 1 and quiescent components, respectively. See text for details.
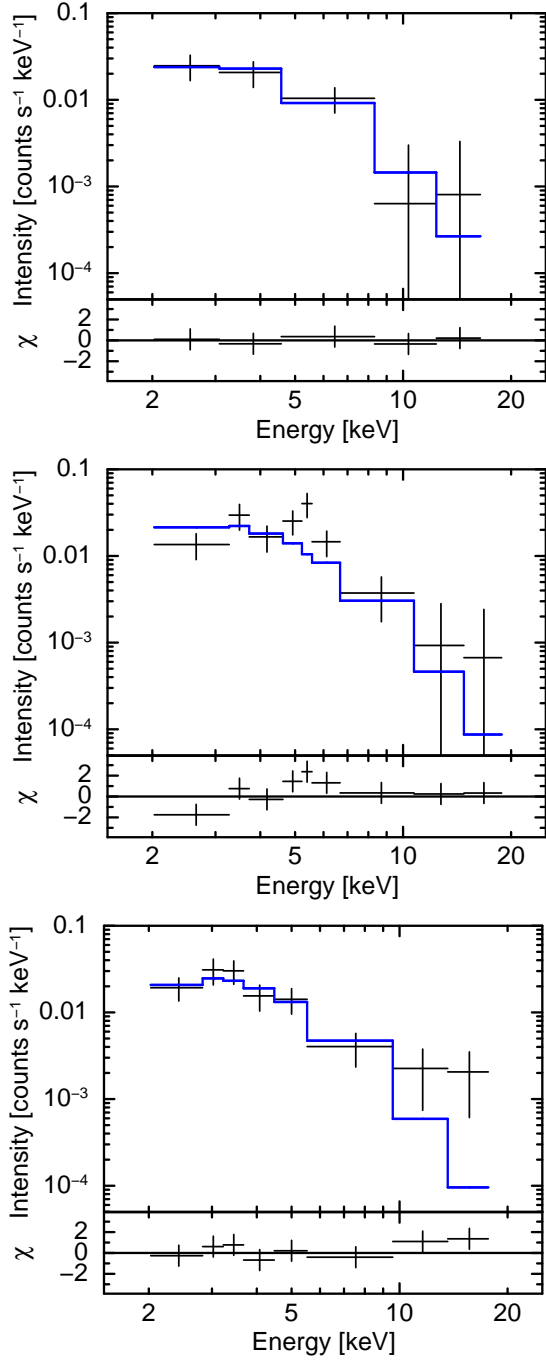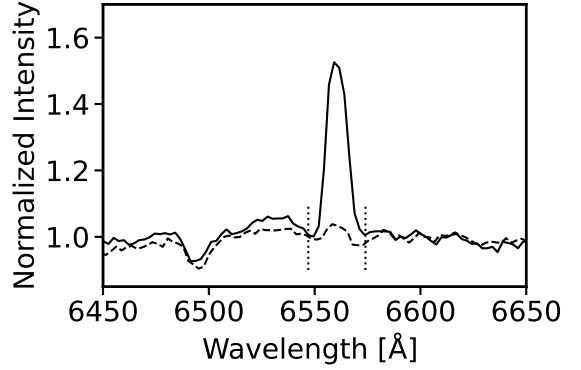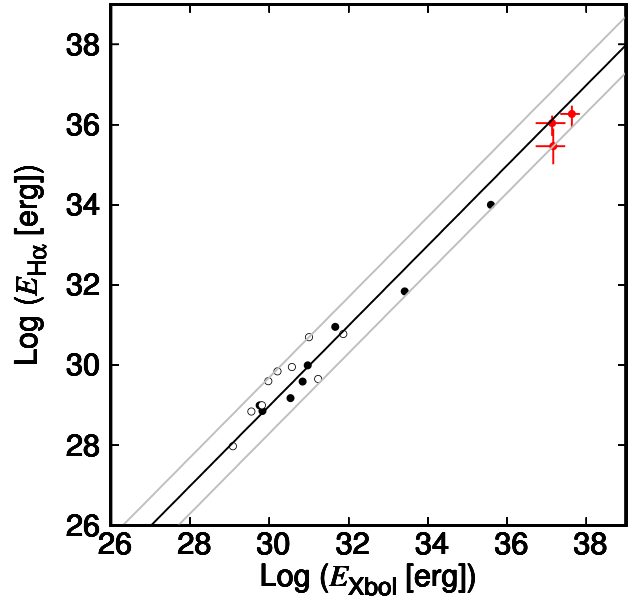

Figure 3: Background-subtracted SXR spectra of Flare 1 (upper panels), Flare 2 (middle), and Flare 3 (lower). The quiescent component is not subtracted. The data points are binned for 2, 6, and 6 MAXI orbits in the respective panels. The errors are in 1σ. The solid lines show the best-fitting models. The residuals for the best-fitting model are also shown at the lower part of each panel.

Figure 5: Log-log plot of radiation energies of Hα and SXR (0.1–100 keV). The open and filled circles in black show the data for the solar and stellar flares found in literature. The red data are our results for the MAXI flares with 90% confidence errors. See text for details. The gray lines indicate 1.6 times of the standard deviation ($\sim$ 90%) of the data points around the model.
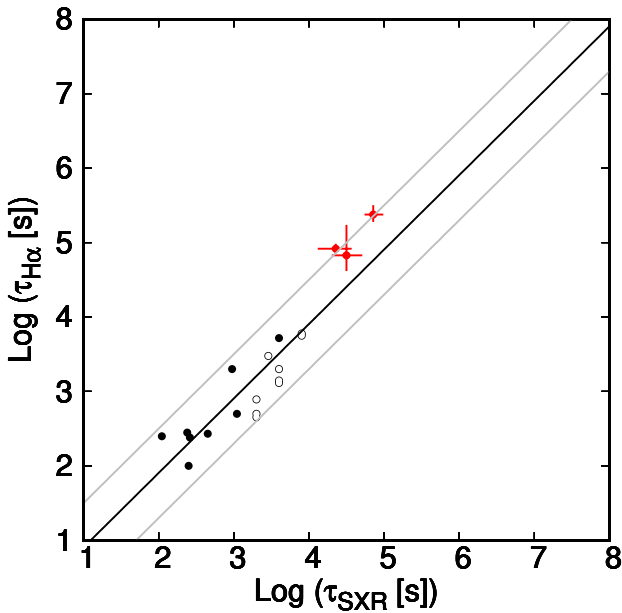
Figure 6: Log-log plot of *e*-folding times of Hα and SXR. The symbols are the same as in Figure 5. The gray lines indicate 1.6 times of the standard deviation (~ 90%) of the data points around the model.

where the error is calculated as the scatter of the data points around the derived model function in 1.6σ.

We find that all the data fall within an factor of 4 around the best-fitting linear function. This result implies that the two parameters τ_{SXR} and $\tau_{\text{H}\alpha}$ are almost the same among not only the solar flares but also much more energetic stellar flares. The result extends the applicable range for the relationship by an order of magnitude from the previous result (Veronig et al., 2002a). It is notable that the overall trend of the data points in the τ_{SXR}-$\tau_{\text{H}\alpha}$ space broadly follows a linear relation for 3 orders of magnitude for the duration τ.

4.4. Solar to large stellar flares

We have found proportional relationships between the SXR and Hα emission line for the flare radiation energy E and e-folding time τ from the solar to large stellar flares. As for the Sun, thanks to the close distance to it, many images have been obtained with high spatial resolution in the Hα emission line and SXR band (e.g. Asai et al., 2004; Jing et al., 2016). SXRs are dominated by optically-thin thermal emission from high-temperature plasma of tens of millions of degrees that fills the loop of each flare (e.g. Shibata and Magara, 2011). The Hα line is, by contrast, found to be emitted near the foot-points of a flare loop and/or from the inner side of SXR flare loop, called post-flare loop (see figure 42 in Shibata and Magara, 2011). The hydrogen responsible for the Hα emission line is thought to be excited by one or all of (1) the collision of accelerated particles, (2) heat conducted from the high-temperature plasma at the foot-point of the flare loop, and (3) the high-energy radiation from the high-temperature plasma. The nominal loop size of the solar flare is reported to be ~ 0.1 $R_{\odot}$ (e.g. Kontar et al., 2011). Although the loop sizes derived for Flares 1 and 2 are

both estimated to be more than twice the stellar radius, our finding of the scaling relationships suggests that the origins of the SXR and Hα of the large flare are common to those of the Sun.

In this work, the studied correlation is limited to Hα and X-rays. Although some studies have been done about the correlation between white light and X-rays, the uncertainty in the results is considerable mainly due to their limited radiated-energy ranges of the sample stellar flares (e.g., Flaccomio et al., 2018; Guarcello et al., 2019; Kuznetsov and Kolotkov, 2021). Future simultaneous observations of stellar flares with X-rays and other bands, including white light, would provide us with insights about the multi-wavelength nature of stellar flares for a wide energy band.

5. Summary

1. During the five years from 2016 October to 2021 September, three large stellar flares from UX Ari and AR Psc were simultaneously observed in Hα and SXRs.

2. The radiation energies of the observed flares were 10^{36}–10^{37} erg in the X-ray band and 10^{35}–10^{36} erg in the Hα emission line. By combining the obtained physical parameters and those in literature for solar and stellar flares, a good proportional relation was obtained between the emitted energies of X-ray and Hα emissions for a flare energy range of 10^{29}–10^{38} erg. This is the first confirmation of the relationship based on simultaneous X-ray and Hα observations of massive stellar flares. The ratio of the Hα line emission to that of SXR is ~0.1, if we take the energy band from 0.1 to 100 keV to obtain the X-ray luminosity.

3. The *e*-folding times in the decay phase of both SXR and Hα flares were obtained to be 10^4–10^5 s. By combining the obtained physical parameters and those in literature for solar and stellar flares, it is confirmed that the *e*-folding times in both bands coincide with the range of 1–10^4 sec.

4. Even very large stellar flares with energies of 6 orders of magnitude larger than the most energetic solar flares follow the same scaling relationships as solar and much less energetic stellar flares. This fact suggests that their physical parameters can be estimated on the basis of the known physics of solar and stellar flares. We stress that this conclusion is derived using the Hα emission data with a limited coverage for flare durations. Future simultaneous observations of SXR and Hα emissions from stellar flares with more complete coverage for the flare duration and with higher statistics will verify the scaling relationships.

Appendix A. Light curves of the four extra flares

We show in Figure A1 the light curves of four flares that are not included in our selection for detailed analysis, out of of the seven flares mentioned in the observations. Flare 4 occurred in UX Ari, Flares 5 and 6, in HR1099, and Flare 7, in VY Ari. All the objects are stars classified as RS CVn type.

Appendix B. Calculation of radiation energies and *e*-folding times from those in literature

The general procedure to calculate the radiation energies and e-folding times in SXRs and Hα (tabulated in table 8) is described in subsections 4.2 and 4.3. In some cases, the values are taken from the cited references as they are presented. However, in many cases, some conversions are required to derive the compiled values (table 8). Here is the detail of the conversion methods. II Peg: E_{Xbol} is calculated from the peak X-ray flux (referred to as $F_{\text{X,peak}}$) and τ_{SXR}, both of which are read directly from a figure in the reference, and $\tau_{H\alpha}$ is read directly from a figure. Glise 644: E_{Xbol} is calculated in a similar manner as that for II Peg except that $F_{\text{X,peak}}$ is taken from a table. YZ CMi with reference (4) in table 8: τ_{SXR} is calculated from a combination of $F_{\text{X,peak}}$ directly read from a figure and energy in reference (7), and $\tau_{H\alpha}$ is from the peak Hα flux ($F_{H\alpha,\text{peak}}$) from a table and $E_{H\alpha}$ in reference (1). YZ CMi with reference (5): τ_{SXR} is from τ_{SXR} calculated from $F_{\text{X,peak}}$ and E_X in reference (5), and $\tau_{H\alpha}$ is directly from a figure. UV Cet: τ_{SXR} is from $F_{\text{X,peak}}$ and τ_{SXR} is directly from a figure and $\tau_{H\alpha}$ from a combination of $F_{H\alpha,\text{peak}}$ directly from a figure and $E_{H\alpha}$ from reference (1). Sun with reference (8): E_{Xbol} is from $F_{\text{X,peak}}$ directly from a figure, and $\tau_{H\alpha}$ is found in the same manner as that for UV Cet. Sun with reference (9): E_{Xbol} is from a combination of $F_{\text{X,peak}}$ directly from a figure and τ_{SXR} from $F_{\text{X,peak}}$ and energy from a table.

References

Agrawal, P.C., Vaidya, J., 1988. Binary phase correlated X-ray intensity variations and flaring in theRS CVn binary HR 1099. MNRAS 235, 239.

Alekseev, I.Y., 2014. Three-Component Model of Spottedness in the Classical RS CVn System UX Ari. Ap 57, 344.

Asai, A., Yokoyama, T., Shimojo, M., Masuda, S., Kurokawa, H., Shibata, K., 2004. Flare Ribbon Expansion and Energy Release Rate. ApJ 611, 557.

Butler, C.J., 1993. An extended correlation between the Balmer and soft X-ray emission from solar and stellar flares. A&A 272, 507.

Butler, C.J., Rodono, M., Foing, B.H., 1988. A correlation between Balmer and soft X-ray emission from stellar & solar flares. A&A 206, L1.

Butler, C.J., Rodono, M., Foing, B.H., Haisch, B.M., 1986. Coordinated Exosat and spectroscopic observations of flare stars and coronal heating. Nature 321, 679.

Carlos, R.C., Popper, D.M., 1971. HD 21242, A Spectroscopic Binary with H and K Emission. PASP 83, 504.

Catalano, S., Umana, G., Cafra, B., Frasca, A., Trigilio, C., Marilli, E., 2003. A Simultaneous Hα and Radio Flare on the RS CVn System UX Ari. in Cambridge Workshop on Cool Stars, Stellar Systems, and the Sun, 12, The Future of Cool-Star Astrophysics, eds , 981.

Doyle, J.G., Butler, C.J., Bryne, P.B., van den Oord, G.H.J., 1988a. Rotational modulation and flares on RS CVn and BY DRA systems. VII. simultaneous X-ray, radio and optical data for the dMe star YZ CMi on 4/5 March 1985. A&A 193, 229.

Doyle, J.G., Butler, C.J., Callanan, P.J., Tagliaferri, G., de La Reza, R., White, N.E., Torres, C.A., Quast, G., 1988b. Rotational modulation and flares on RS CVn and BY DRA systems. VIII. Simultaneous EXOSAT and H alpha observations of a flare on the dMe star GL 644 AB (Wolf 630) on 24/25 August 1985. A&A 191, 79.

Doyle, J.G., Kellett, B.J., Byrne, P.B., Avgoloupis, S., Mavridis, L.N., Seiradakis, J.H., Bromage, G.E., Tsuru, T., Makishima, K., Makishima, K., McHardy, I.M., 1991. Simultaneous detection of a large flare in the X-ray and optical regions on the RS CVn-type star II Peg. MNRAS 248, 503.

ESA, 1997. The HIPPARCOS and TYCHO catalogues. Astrometric and photometric star catalogues derived from the ESA HIPPARCOS Space Astrometry Mission. ESA Special Publication, 1200 1200.

Fekel, F.C., 1996. Chromospherically Active Stars. XV. HD 8357=AR Piscium, an Extremely Active RS CVn System. AJ 112, 269.

Fekel, F.C., Moffett, T.J., Henry, G.W., 1986. A Survey of Chromospherically Active Stars. ApJS 60, 551.

Feldman, P.A., 1978. Large Radio Flares in RS CVn Binaries. BAAS 10, 418.

Flaccomio, E., Micela, G., Sciortino, S., Cody, A.M., Guarcello, M.G., Morales-Calderòn, M., Rebull, L., Stauffer, J.R., 2018. A multi-wavelength view of magnetic flaring from PMS stars. A&A 620, 55.

Fuhrmeister, B., Lalitha, S., Poppenhaeger, K., Rudolf, N., Liefke, C., Reiners, A., Schmitt, J.H.M.M., Ness, J.U., 2011. Multi-wavelength observations of Proxima Centauri. A&A 534, 133.

Gaia Collaboration, Brown, A.G.A., Vallenari, A., Prusti, T., de Bruijne, J.H.J., Babusiaux, C., Bailer-Jones, C.A.L., Biermann, M., Evans, D.W., Eyer, L., Jansen, F., et al., 2018. Gaia Data Release 2. Summary of the contents and survey properties. A&A 616, A1.

Garcia, M., Baliunas, S.L., Conroy, M., Johnston, M.D., Ralph, E., Roberts, W., Schwartz, D.A., Tonry, J., 1980. Optical identification of H 0123+07.5 and 4U 1137-65 : hard X-ray emission from RS CVn systems. ApJ Vol. 240, 107.

Guarcello, M.G., Micela, G., Sciortino, S., López-Santiago, J., Argiroffi, C., Reale, F., Flaccomio, E., Alvarado-Gómez, J.D., Antoniou, V., et al., 2019. Simultaneous Kepler/K2 and XMM-Newton observations of superflares in the Pleiades. A&A 622, 210.

Haisch, B.M., 1983. X-ray observations of stellar flares. in IAU Colloq. 71, Activity in Red-Dwarf Stars, ed. P. B. Byrne & M. Rodono (Dordrecht: Reidel) , 255.

Hummel, C.A., Monnier, J.D., Roettenbacher, R.M., Torres, G., Henry, G.W., Korhonen, H., Beasley, A., Schaefer, G.H., Turner, N.H., Ten Brummelaar, T., 2017. Orbital Elements and Stellar Parameters of the Active Binary UX Arietis. ApJ 844, 115.

Jing, J., Xu, Y., Cao, W., Liu, C., Gary, D., Wang, H., 2016. Unprecedented Fine Structure of a Solar Flare Revealed by the 1.6 m New Solar Telescope. NatSR 6, 24319.

Johns-Krull, C.M., Hawley, S.L., Basri, G., Valenti, J.A., 1997. Hamilton Echelle Spectroscopy of the 1993 March 6 Solar Flare. ApJS 112, 221.

Kahler, S., Golub, L., Harnden, F.R., Liller, W., Seward, F., Vaiana, G., Lovell, B., Davis, R.J., Spencer, R.E., Whitehouse, D.R., Feldman, P.A., Viner, M.R., Leslie, B., Kahn, S.M., Mason, K.O., Davis, M.M., Crannell, C.J., Hobbs, R.W., Schneeberger, T.J., Worden, S.P., Schommer, R.A., Vogt, S.S., Pettersen, B.R., Coleman, G.D., Karpen, J.T., Giampapa, M.S., Hege, E.K., Pazzani, V., Rodono, M., Romeo, G., Chugainov, P.F., 1982. Coordinated X-ray, optical and radio observations of flaring activityon YZ Canis Minoris. ApJ 252, 239.

Kashapova, L.K., Broomhall, A., Larionova, A.I., Kupriyanova, E.G., Motyk, I.D., 2021. The morphology of average solar flare time profiles from observations of the Sun's lower atmosphere. MNRAS 502, 3922.

Kashyap, V., Drake, J.J., 1999. On X-Ray Variability in Active Binary Stars. ApJ 524, 988–999.

Kawagoe, A., Tsuboi, Y., Negoro, H., Kawai, N., Sakamoto, T., Nakahira, S., Serino, M., Ueno, S., Tomida, H., Kimura, M., Nakagawa, Y.E., Mihara, T., Sugizaki, M., Morii, M., Sugimoto, J., Takagi, T., Yoshikawa, A., Matsuoka,
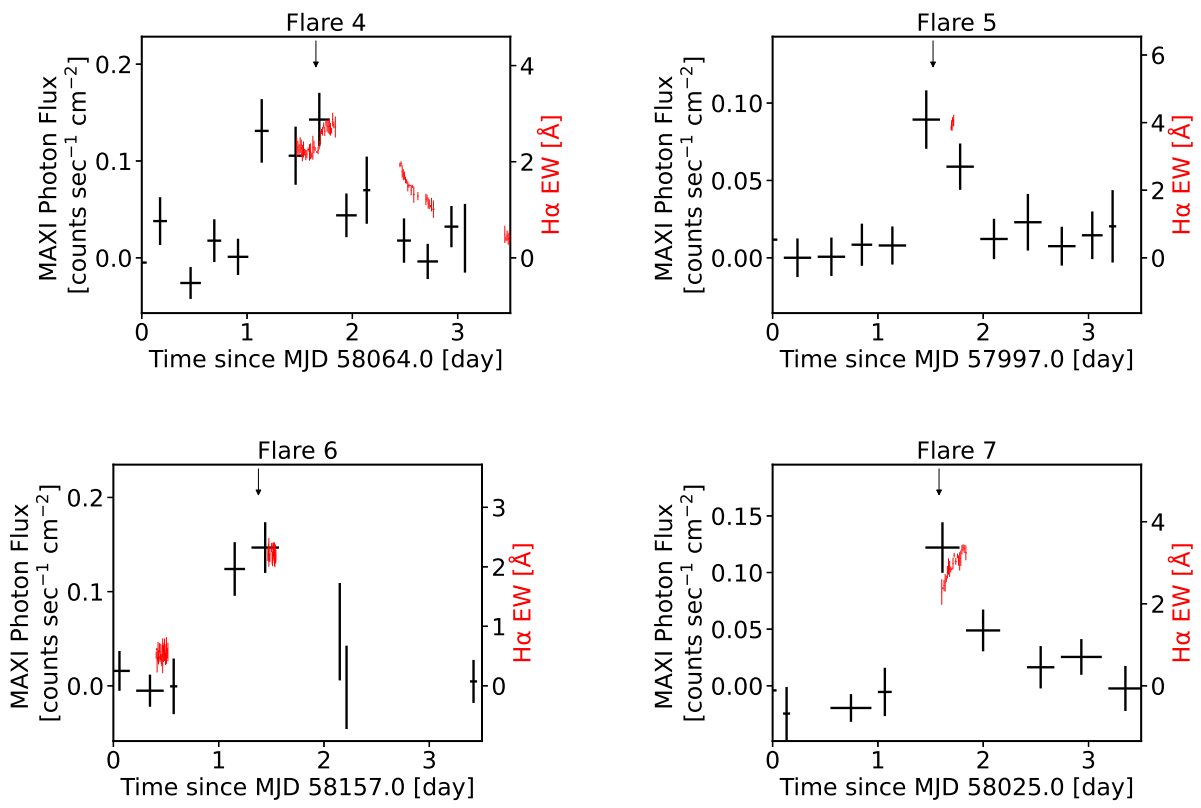
Figure A1: SXR and Hα light curves of four of the seven flares that are not discussed in the main text: Flares 4 (upper left), 5 (upper right), 6 (lower left), and 7 (lower right). The downward arrow indicates the time of flare detection by "nova search" for each flare.

M., Usui, R., Yoshii, T., et al., 2014. MAXI/GSC detection of a big flare from UX Ari. ATel 6315.

Kontar, E.P., Hannah, I.G., Bian, N.H., 2011. Acceleration, Magnetic Fluctuations, and Cross-field Transport of Energetic Electrons in a Solar Flare Loop. ApJL 730, 22.

Kuznetsov, A.A., Kolotkov, D.Y., 2021. Stellar Superflares Observed Simultaneously with Kepler and XMM-Newton. ApJ 912, 81.

Massi, M., Neidhofer, J., Torricelli-Ciamponi, G., Chiuderi-Drago, F., 1998. Activity cycles in UX ARIETIS. A&A 332, 149.

Massi, M., Neidhöfer, J., Carpentier, Y., Ros, E., 2005. Discovery of Solar Rieger periodicities in another star. A&A 435, 1.

Massi, M., Ros, E., 2002. Investigation of magnetic loop structures in the corona of UX Arietis. 6th European VLBI Network Symposium on New Developments in VLBI Science and Technology , 275.

Matsumura, T., Tsuboi, Y., Yamazaki, K., Morii, M., Ueno, S., Tomida, H., Kohama, M., Ishikawa, M., Mihara, T., Sugizaki, M., Serino, M., Nakahira, S., Yamamoto, T., Sootome, T., Matsuoka, M., Kawai, N., Sugimori, K., Usui, R., Toizumi, T., Yoshida, A., et al., 2011. MAXI/GSC detection of an active state of the RS CVn type star UX Ari. ATel 3308.

Matsuoka, M., Kawasaki, K., Ueno, S., Tomida, H., Kohama, M., Suzuki, M., Adachi, Y., Ishikawa, M., Mihara, T., Sugizaki, M., Isobe, N., Nakagawa, Y., Tsunemi, H., Miyata, E., Kawai, N., Kataoka, J., Morii, M., Yoshida, A., Negoro, H., Nakajima, M., Ueda, Y., Chujo, H., Yamaoka, K., Yamazaki, O., Nakahira, S., You, T., Ishiwata, R., Miyoshi, S., Eguchi, S., Hiroi, K., Katayama, H., Ebisawa, K., 2009. The MAXI Mission on the ISS: Science and Instruments for Monitoring All-Sky X-Ray Images. PASJ 61, 999. arXiv:0906.0631.

Mihara, T., Nakajima, M., Sugizaki, M., Serino, M., Matsuoka, M., Kohama, M., Kawasaki, K., Tomida, H., Ueno, S., Kawai, N., Kataoka, J., Morii, M., Yoshida, A., Yamaoka, K., Nakahira, S., Negoro, H., Isobe, N., Yamauchi, M., Sakurai, I., 2011. Gas Slit Camera (GSC) onboard MAXI on ISS. PASJ 63, 623–634. arXiv:1103.4224.

Nakahira, S., Ebisawa, K., Negoro, H., 2013. Development of the MAXI/GSC all-sky data archive system. JAXA Research and development report: Journal of Space Science Informatics Japan 2, 29.

Nakamura, Y., Tsuboi, Y., Sasaki, R., Serino, M., Nakahira, S., Ueno, S., Tomida, H., Ishikawa, M., Nakagawa, Y.E., Sugawara, Y., Mihara, T., Sugizaki, M., Iwakiri, W., Shidatsu, M., Sugimoto, J., Takagi, T., Matsuoka, M., Kawai, N., Isobe, N., Sugita, S., et al., 2016. MAXI/GSC detection of a possible X-ray flare from an RS CVn star AR Psc. ATel 9288.

Namekata, K., Maehara, H., Sasaki, R., Kawai, H., Notsu, Y., Kowalski, A.F., Allred, J.C., Iwakiri, W., et al., 2020. Optical and X-ray observations of stellar flares on an active M dwarf AD Leonis with the Seimei Telescope, SCAT, NICER, and OISTER. PASJ 72, 68.

Negoro, H., Kohama, M., Serino, M., Saito, H., Takahashi, T., Miyoshi, S., Ozawa, H., Suwa, F., Asada, M., Fukushima, K., Eguchi, S., Kawai, N., Kennea, J., Mihara, T., Morii, M., Nakahira, S., Ogawa, Y., Sugawara, A., Tomida, H., Ueno, S., Ishikawa, M., Isobe, N., Kawamuro, T., Kimura, M., Masumitsu, T., Nakagawa, Y.E., Nakajima, M., Sakamoto, T., Shidatsu, M., Sugizaki, M., Sugimoto, J., Suzuki, K., Takagi, T., Tanaka, K., Tsuboi, Y., Tsunemi, H., Ueda, Y., Yamaoka, K., Yamauchi, M., Yoshida, A., Matsuoka, M., 2016. The MAXI/GSC Nova-Alert System and results of its first 68 months. PASJ 68, 1.

Peterson, W.M., Mutel, R.L., Lestrade, J.F., Güdel, M., Goss, W.M., 2011. Radio Astrometry of the Triple Systems Algol and UX Arietis. ApJ 737, 104.

Sasaki, R., Tsuboi, Y., Iwakiri, W., Nakahira, S., Maeda, Y., Gendreau, K., Corcoran, M.F., Hamaguchi, K., Arzoumanian, Z., Markwardt, C.B., Enoto, T., Sato, T., Kawai, H., Mihara, T., Shidatsu, M., Negoro, H., Serino, M., 2021. The RS CVn-type Star GT Mus Shows Most Energetic X-Ray Flares Throughout the 2010s. ApJ 910, 25. arXiv:2103.16822.

Sasaki, R., Tsuboi, Y., Katsuda, S., Yabuki, K., Nakamura, Y., Sugawara, Y., Matsuoka, M., Team, M., 2017. A Correlation on Stellar Flares detected with MAXI Quiescent Luminosity vs. Flare Energy. The X-ray Universe 2017, Proceedings of the conference held 6-9 June, 2017 in Rome, Italy. Edited by J.-U. Ness and S. Migliari. 201.

Shan, H., Liu, X., Gu, S., 2006. The atmospheric parameters, abundances and magnetic field of the AR piscium primary. New Astron. 11, 287–292.

Shibata, K., Magara, T., 2011. Solar Flares: Magnetohydrodynamic Processes. Living Rev. Sol. Phys. 8, 6.

Shibata, K., Yokoyama, T., 1999. Origin of the Universal Correlation between the Flare Temperature and the Emission Measure for Solar and Stellar Flares. ApJ 526, L49.

Smith, R.K., Brickhouse, N.S., Liedahl, D.A., Raymond, J.C., 2001. Collisional Plasma Models with APEC/APED: Emission-Line Diagnostics of Hydrogen-like and Helium-like Ions. ApJ 556, 91. arXiv:astro-ph/0106478.

Thomas, R.J., Teske, R.G., 1971. Solar Soft X-Rays and Solar Activity. II: Soft X-Ray Emission during Solar Flares. Sol. Phys. 16, 431.

Tsuboi, Y., Koyama, K., Murakami, H., Hayashi, M., Skinner, S., Ueno, S., 1998. ASCA Detection of a Superhot 100 Million K X-Ray Flare on the Weak-Lined T Tauri Star V773 Tauri. ApJ 503, 894.

Tsuboi, Y., Yamazaki, K., Sugawara, Y., Kawagoe, A., Kaneto, S., Iizuka, R., Matsumura, T., Nakahira, S., et al., 2016. Large X-ray flares on stars detected with MAXI/GSC: A universal correlation between the duration of a flare and its X-ray luminosity. PASJ 68, 90. arXiv:1609.01925.

Tsuru, T., Makishima, K., Ohashi, T., Inoue, H., Koyama, K., Turner, M.J.L., Barstow, M.A., McHardy, I.M., Pye, J.P., Tsunemi, H., Kitamoto, S., Taylor, A.R., Nelson, R.F., 1989. X-ray and radio observations of flares from the RS Canum Venaticorum system UX Arietis. PASJ 41, 679.

Veronig, A., Temmer, M., Hanslmeier, A., Messerotti, M., Otruba, W., Moretti, P.F., 2002a. Temporal characteristics of solar soft X-ray and Hα flares. Proceedings of the Second Solar Cycle and Space Weather Euroconference 477, 187.

Veronig, A., Vršnak, B., Temmer, M., Hanslmeier, A., 2002b. Relative timing of solar flares observed at different wavelengths. Sol. Phys. 208, 297.

Webb, N.A., Coriat, M., Traulsen, I., Ballet, J., Motch, C., Carrera, F.J., Koliopanos, F., Authier, J., et al., 2020. The XMM-Newton serendipitous survey. IX. The fourth XMM-Newton serendipitous source catalogue. A&A 641, 136.